Phase separation in an exactly solvable model binary solution with three-body interactions and intermolecular bonding

Radu P. Lungu,* Dale A. Huckaby,† and Florin D. Buzatu‡
Department of Chemistry, Texas Christian University, Fort Worth, Texas 76129, USA
(Received 5 February 2005; revised manuscript received 31 October 2005; published 24 February 2006)

A model is presented in which the bonds of a honeycomb lattice are covered by rodlike molecules of types *AA* and *BB*, molecular ends near a common site having both three-body interactions and orientation-dependent bonding between two *A* molecular ends and between an *A* and a *B* molecular end. Phase diagrams corresponding to the separation into *AA*-rich and *BB*-rich phases are calculated exactly. Depending on the relative strengths of the interactions, one of several qualitatively different types of phase diagrams can result, including diagrams containing phenomena such as a double critical point or two separate asymmetric closed loops. The model is essentially a limiting case of a previously considered ternary solution model, and it is equivalent to a two-component system of interacting *A* and *B* molecules on the sites of a kagomé lattice.

DOI: 10.1103/PhysRevE.73.021508 PACS number(s): 64.70.Ja, 05.70.Fh, 05.50.+q, 64.60.Kw

I. INTRODUCTION

Statistical-mechanical lattice models have been used for many years to model phase transitions in binary and ternary liquid systems. One particularly interesting type of phase diagram, the closed-loop phase diagram, results if the components of a binary liquid system are completely miscible at low temperatures, separate into two phases at moderate temperatures, and are again completely miscible at sufficiently high temperatures. The low-temperature miscibility is usually due to the energetic favorableness of directional intermolecular bonding interactions between unlike molecules, the separation at moderate temperatures is then due to the increasing entropic importance of the large number of intermolecular orientations associated with repulsive interactions rather than bonding, and thermal mixing finally occurs at sufficiently high temperatures.

A closed-loop diagram contains both an upper and a lower critical point, and if the amount of an added third component is varied, the two critical points become lines on a coexistence surface that can coincide at a double critical point. The presence of three-body interactions can cause other interesting effects, including asymmetries in the shape of coexistence surfaces. Exactly solvable models are extremely valuable for studying these types of systems, for the shapes of the resulting phase diagrams can be accurately obtained, even in the neighborhood of critical points.

We recently constructed and studied an exactly solvable model of a ternary solution containing three-body interactions that exhibits closed-loop phase diagrams and double critical points [1]. The model is a generalization of a ternary solution model introduced by Wheeler and Widom [2], in which the links of a honeycomb lattice are occupied by bifunctional rodlike molecules with ends of type *A* or *B*. The model includes three-body interactions between a triangle of neighboring molecular ends, including state-dependent bonding interactions between neighboring pairs of molecular ends in the triangle.

In the model originally studied by Wheeler and Widom [2], unlike ends near a common site experience infinite repulsion, and the model is isomorphic to a standard spin-1/2 Ising model on the lattice, its ferromagmetic transition corresponding to phase separation in the ternary solution. For several generalizations of the Wheeler-Widom model on the honeycomb, square, or Bethe lattices, the coexistence surface for separation into *AA*-rich and *BB*-rich phases has been calculated exactly. These generalizations include the introduction first of finite two-body interactions between pairs of molecular ends near a common site [3–6], followed by the generalization of the model to incorporate three-body interactions [7,8]. Another generalization involved the inclusion of bonding and nonbonding states at the molecular ends to describe orientation-dependent hydrogen bonding, first by considering only two-body interactions [9,10] and then by considering three-body interactions [1]. In these cases two-phase coexistence surfaces that contain double critical points were calculated exactly. In addition to *AA*-rich and *BB*-rich phases, the model can also have ordered *AB*-rich phases, and this aspect has been studied with infinite repulsion between unlike neighboring ends [2,11], with generalizations of this restricted version [12–14], with finite two-body interactions [15], and with four types of molecular ends [16–18]. The model has also been used to calculate the spinodal curve [19].

In Sec. II of the present paper we construct a generalized Wheeler-Widom molecular model for a binary solution that contains molecules of types *AA* and *BB* on a honeycomb lattice. The model can also be formulated as a ternary solution model, with the binary solution resulting as a limiting case. The present model is similar to the binary solution limit of the model considered in Ref. [1], but it differs in two aspects. First, it is generalized energetically to incorporate

*Permanent address: Department of Physics, University of Bucharest, Bucharest-Magurele 76900, Romania.
†Electronic address: d.huckaby@tcu.edu
‡Permanent address: Department of Theoretical Physics, National Institute for Physics and Nuclear Engineering, Bucharest-Magurele 76900, Romania.

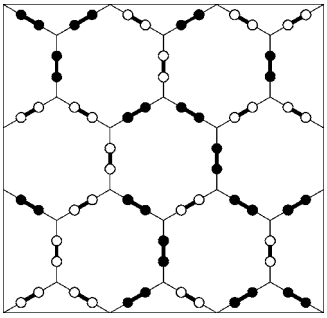

FIG. 1. A configuration of molecules on the honeycomb lattice, where molecular ends of type A are depicted as white disks and those of type B as black disks.

more types of intermolecular bonding interactions, resulting in a richer variety of possible phase diagrams, including ones that contain one or both of a low-temperature coexistence curve and an intermediate-temperature closed loop, or even two closed loops. Second, in the present model the internal states, or orientations, are considered and counted as being associated with each portion of a molecular end that faces a neighboring end [9,10], whereas in Ref. [1] the internal states are associated with the entire molecular end. In addition to containing many interesting types of coexistence curves, the temperature-composition phase diagrams of the binary solution model are two dimensional and are thus more convenient to study than would be the three-dimensional phase diagrams of the corresponding ternary solution model that also contains molecules of type AB.

In Sec. III exact equations are obtained for the two-phase coexistence diagrams in temperature-composition space. Since the generalized binary solution model contains 20 parameters, it is difficult to study in detail; for this reason, in Sec. IV we consider a simplified version of the generalized model that has only six effective adjustable parameters, each having a physical meaning. Then, by fixing four of the parameters and varying the other two, we calculated exact phase diagrams that contain the full variety of possible features.

II. THE MODEL

In the following we consider a binary solution, composed of rodlike molecules of types AA and BB, and described by a lattice model which can be considered a generalized Wheeler-Widom molecular model.

The model is based on the following assumptions.

(A1) Every link connecting two neighboring sites of a honeycomb lattice is occupied by one rodlike molecule of type AA or BB. Illustrated in Fig. 1 is a portion of the honeycomb lattice having molecules on the links.

(A2) The triangle of molecular ends X, Y, and Z (this means AAA, BBB, ABA, or BAB) near a lattice site of the honeycomb lattice experiences state-dependent three-body interactions. The portion of molecular end X that faces molecular end Y can be in any one of q_X states (representing local orientations), one of which is a bonding state. If the portion of molecular end Y that faces X is also in a bonding state, a bond forms between X and Y. There are thus $q_X q_Y$ pair states associated with the pair of ends X and Y (and similarly for the pair X and Z and the pair Y and Z), one of which is bonding, the other $q_X q_Y - 1$ of which are free states (nonbonding). If bonding is considered to be forbidden between two specific types of neighboring ends, this case can be considered as a special case of the above in which the bond contributes no energy.

TABLE I. Weights for an XXX triangle.

Weight	Bonds
$c_{XXX}^{(0)}=\left(1-\frac{1}{q_X^2}\right)^3$	No bonds
$c_{XXX}^{(1)}=\frac{3}{q_X^2}\left(1-\frac{1}{q_X^2}\right)^2$	$\overline{XX}$
$c_{XXX}^{(2)}=\frac{3}{q_X^4}\left(1-\frac{1}{q_X^2}\right)$	$2\overline{XX}$
$c_{XXX}^{(3)}=\frac{3}{q_X^6}$	$3\overline{XX}$

If we denote by $z_{XYZ}^{(r)}$ the number of states for an XYZ triangle with bonding of type r, then $z_{XYZ}=\Sigma_r z_{XYZ}^{(r)}=q_X^2 q_Y^2 q_Z^2$ is the total number of possible states for the triangle. Then $c_{XYZ}^{(r)}=z_{XYZ}^{(r)}/z_{XYZ}$ is the weight of states with bonding of type r. The weights for the XXX triangles (AAA or BBB) are given in Table I, and the weights for the XYX triangles (ABA or BAB) are given in Table II.

The three-body energy associated with a triangle of molecular ends X, Y, and Z, having bonding of type r, will be denoted $\varepsilon_{XYZ}^{(r)}$. For convenience, we classify the set of states of a triangle as being *pure states* if no bonds are present and as being *bonding states* if one or more bonds are present. We can then decompose the energy $\varepsilon_{XYZ}^{(r)}$ into the energy $\varepsilon_{XYZ}^{(0)}$ of a pure state and the supplementary energy $\delta\varepsilon_{XYZ}^{(r)}$ due to the bonds as

$$\varepsilon_{XYZ}^{(r)}=\varepsilon_{XYZ}^{(0)}+\delta\varepsilon_{XYZ}^{(r)}. \tag{2.1}$$

In addition, we use the following completely equivalent *two-body-like* representation for the three-body energies of the free states:

TABLE II. Weights for an XYX triangle.

Weight	Bonds
$c_{XYX}^{(0)}=\left(1-\frac{1}{q_X^2}\right)\left(1-\frac{1}{q_X q_Y}\right)^2$	No bonds
$c_{XYX}^{(1;XX)}=\frac{1}{q_X^2}\left(1-\frac{1}{q_X q_Y}\right)^2$	$\overline{XX}$
$c_{XYX}^{(1;XY)}=\frac{2}{q_X q_Y}\left(1-\frac{1}{q_X^2}\right)\left(1-\frac{1}{q_X q_Y}\right)$	$\overline{XY}$
$c_{XYX}^{(2;XX,XY)}=\frac{2}{q_X^3 q_Y}\left(1-\frac{1}{q_X q_Y}\right)$	$\overline{XX}+\overline{XY}$
$c_{XYX}^{(2;XY)}=\frac{2}{q_X^2 q_Y^2}\left(1-\frac{1}{q_X^2}\right)$	$2\overline{XY}$
$c_{XYX}^{(3)}=\frac{1}{q_X^4 q_Y^2}$	$2\overline{XY}+\overline{XX}$

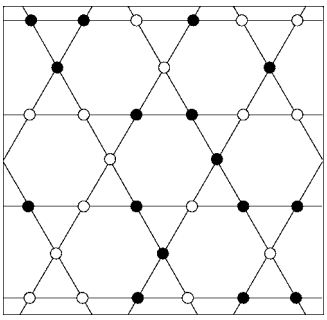

FIG. 2. The kagomé lattice, obtained by shrinking the molecules to points; the A molecules are depicted as white disks and the B molecules as black disks.

$$\begin{cases} \varepsilon_{XXX}^{(0)} = 3\epsilon_{XX} & \text{for an } AAA \text{ or } BBB \text{ triangle}, \\ \varepsilon_{XYX}^{(0)} = \epsilon_{XX} + 2\epsilon_{XY} & \text{for an } ABA \text{ or } BAB \text{ triangle}. \end{cases} \tag{2.2}$$

(In the limiting case of two-body interactions, ϵ_{XX} and $\epsilon_{XY} = \epsilon_{YX}$ become the interaction energies between XX and XY molecular ends.)

The *average energy* $\bar{\varepsilon}_{XYZ}$ of a bonding state for an XYZ triangle is then defined by

$$e^{-\beta\bar{\varepsilon}_{XYZ}} = \sum_r c_{XYZ}^{(r)} e^{-\beta\varepsilon_{XYZ}^{(r)}}, \tag{2.3}$$

where $\beta \equiv 1/(k_B T)$, with k_B being Boltzmann's constant and T being the temperature. Using the decomposition of the energies expressed by Eq. (2.1), we factor the bonding contribution in the average energy,

$$e^{-\beta\bar{\varepsilon}_{XYZ}} = \omega_{XYZ} e^{-\beta\varepsilon_{XYZ}^{(0)}}, \tag{2.4}$$

where the characteristic function ω_{XYZ} is given as

$$\omega_{XYZ} = \sum_r c_{XYZ}^{(r)} e^{-\beta\delta\varepsilon_{XYZ}^{(r)}}. \tag{2.5}$$

The finite honeycomb lattice with periodic boundaries, having N_t sites (where $2t$ is the minimum length of a cycle that is not homotopic to a point), is denoted as G_t; in addition, we introduce the associated kagomé lattice, denoted as Λ_t, which has vertices at the positions of the centers of molecules [20,21]; thus, the kagomé lattice is covered by C_3 graphs (the triangles). The kagomé lattice is illustrated in Fig. 2.

A microscopic configuration of the whole molecular system, ξ, is completely specified by the configuration of the molecular ends (defined by the set of occupancy numbers $\{P\}$ on all the sites of Λ_t) and the set of the internal state types $\{\alpha\}$ for all the triangles. Then, the grand-canonical Hamiltonian for the generalized model on Λ_t, having the configuration ξ, is

$$\mathcal{H}_{\Lambda_t}(\xi) = \sum_{\substack{X,Y,Z\in\{A,B\} \\ \langle i,j,k\rangle\subset C_3}} \varepsilon_{XYZ}^{\alpha} P_i^X P_j^Y P_k^Z - \sum_{\substack{X\in\{A,B\} \\ i\in\Lambda_t}} \mu_{XX} P_i^X, \tag{2.6}$$

where P_j^X is an occupation number defined as [7]

$$P_j^X(\xi) = \begin{cases} 1, & \text{if on } j \in \Lambda_t \text{ is an } X\text{-type end in } \xi, \\ 0, & \text{otherwise}. \end{cases}$$

The corresponding grand-canonical partition function is then obtained by summing over all possible configurations:

$$\Xi_{\Lambda_t} = \sum_{\xi} e^{-\beta\mathcal{H}_{\Lambda_t}(\xi)}. \tag{2.7}$$

We note that, in order to avoid the contribution of configurations containing vacancies, we shall consider the limit of infinite chemical potentials ($\mu_{AA} \to \infty$ and $\mu_{BB} \to \infty$), but with the restriction that their difference remain finite.

In order to obtain the correspondence between the grand-canonical partition function of the molecular system and the canonical partition function of a simple Ising model, we realize in succession the following steps.

(a) First we perform the summations over internal states, and it results in a grand-canonical partition function, which is formally the same as that for a molecular model without internal states but with temperature-dependent energies,

$$\Xi_{\Lambda_t} = \sum_{\{P\}} e^{-\beta\bar{\mathcal{H}}_{\Lambda_t}\{P\}}, \tag{2.8}$$

where $\bar{\mathcal{H}}_{\Lambda_t}\{P\}$ is *the averaged grand-canonical Hamiltonian*:

$$\bar{\mathcal{H}}_{\Lambda_t}\{P\} = \sum_{\substack{X,Y,Z\in\{A,B\} \\ \langle i,j,k\rangle\subset C_3}} \left[\bar{\varepsilon}_{XYZ} - \frac{1}{\beta}\ln(z_{XYZ})\right] P_i^X P_j^Y P_k^Z - \sum_{\substack{X\in\{A,B\} \\ i\in\Lambda_t}} \mu_{XX} P_i^X. \tag{2.9}$$

(b) Since in Eqs. (2.8) and (2.9) we have formally no internal states, we can use the spin representation of the occupancy numbers $P_j^{A/B} = (1 \pm S_j)/2$, where $S_j = \pm 1$ if site $j \in \Lambda_t$ is occupied by an A/B-type molecular end; then, the grand-canonical partition function of the molecular model (Ξ_{Λ_t}) becomes proportional to the canonical partition function of the Ising model on the kagomé lattice (Z_{Λ_t}):

$$\Xi_{\Lambda_t} = e^{-\beta K_I} Z_{\Lambda_t}, \tag{2.10}$$

where

$$Z_{\Lambda_t}(R_3, R, h) = \sum_{\{S_i\}_{i\in\Lambda_t}} \exp\left\{ R_3 \sum_{\langle i,j,k\rangle\subset C_3} S_i S_j S_k + R \sum_{\langle i,j\rangle\subset C_3} S_i S_j + h \sum_{i\in\Lambda_t} S_i \right\} \tag{2.11}$$

and the reduced Ising parameters, together with the constant K_I, are given by

$$R_3 = \frac{\beta}{8}(3\bar{\varepsilon}_{ABA} - 3\bar{\varepsilon}_{BAB} - \bar{\varepsilon}_{AAA} + \bar{\varepsilon}_{BBB}), \tag{2.12}$$

$$R = \frac{\beta}{8}(\bar{\varepsilon}_{ABA} + \bar{\varepsilon}_{BAB} - \bar{\varepsilon}_{AAA} - \bar{\varepsilon}_{BBB}), \tag{2.13}$$

$$h = \frac{\beta}{8}[(-\bar{\varepsilon}_{ABA} + \bar{\varepsilon}_{BAB} - \bar{\varepsilon}_{AAA} + \bar{\varepsilon}_{BBB}) + 2(\mu_{AA} - \mu_{BB})] + \ln\left(\frac{q_A}{q_B}\right), \tag{2.14}$$

$$K_I = \left\{\frac{1}{8}(\bar{\varepsilon}_{AAA} + \bar{\varepsilon}_{BBB} + 3\bar{\varepsilon}_{ABA} + 3\bar{\varepsilon}_{BAB}) - \frac{1}{2}(\mu_{AA} + \mu_{BB}) - \frac{3}{\beta}\ln(q_A q_B)\right\} 3N_t. \tag{2.15}$$

We present some necessary comments concerning the previous results.

(1) The constant K_I is independent of the spin configuration and therefore has no contribution to the description of a phase transition.

(2) Using Eq. (2.4), we obtain the decompositions of the Ising parameters R_3 and R into pure-state contributions (common to all the models for bonding) and the supplementary bonding contributions:

$$R_3 = \frac{\beta}{4}3(\epsilon_{AB} - \epsilon_{BA}) + \frac{1}{8}\ln\left[\frac{\omega_{AAA}\omega_{BAB}^3}{\omega_{BBB}\omega_{ABA}^3}\right], \tag{2.16}$$

$$R = \frac{\beta}{4}(\epsilon_{AB} + \epsilon_{BA} - \epsilon_{AA} - \epsilon_{BB}) + \frac{1}{8}\ln\left[\frac{\omega_{AAA}\omega_{BBB}}{\omega_{ABA}\omega_{BAB}}\right]. \tag{2.17}$$

(3) Equations (2.16), (2.17), and (2.5) lead to a dimensionless form of the whole problem if we choose as a standard energy the quantity $\epsilon_0 \equiv \epsilon_{AB} + \epsilon_{BA} - \epsilon_{AA} - \epsilon_{BB}$ and then define the *reduced temperature* (τ) and the *reduced energetic parameters* Δ and $\{k_{XYZ}^{(r)}\}$, as

$$\beta\epsilon_0 = \frac{4}{\tau}, \tag{2.18}$$

$$\Delta = \frac{3(\epsilon_{AB} - \epsilon_{BA})}{\epsilon_0}, \tag{2.19}$$

$$k_{XYZ}^{(r)} = \frac{-\delta\varepsilon_{XYZ}^{(r)}}{\epsilon_0} \tag{2.20}$$

(for physical bonding, $\delta\varepsilon_{XYZ}^{(r)} < 0$, resulting in $k_{XYZ}^{(r)} > 0$). Then, the dimensionless form of the Ising parameters for the model is

$$R_3 = \frac{\Delta}{\tau} + \frac{1}{8}\sum_j \chi_j \ln(\omega_j), \tag{2.21}$$

$$R = \frac{1}{\tau} + \frac{1}{8}\sum_j \gamma_j \ln(\omega_j), \tag{2.22}$$

where the summations imply $j \in \{AAA, BBB, ABA, BAB\}$ and the coefficients are $\chi_{AAA} = -\chi_{BBB} = 1$, $\chi_{BAB} = -\chi_{ABA} = 3$, and $\gamma_{AAA} = \gamma_{BBB} = -\gamma_{ABA} = -\gamma_{BAB} = 1$; also, the characteristic function of the triangle, in dimensionless form, is

$$\omega_{XYZ} = \sum_r c_{XYZ}^{(r)} e^{4k_{XYZ}^{(r)}/\tau}. \tag{2.23}$$

(We note that for pure states $\omega_{XYZ} = 1$.)

(4) If we denote the maximum reduced energetic parameter as $k_j^M \equiv \max_r(k_j^{(r)})$ and the corresponding weight as c_j^M, the asymptotic behaviors of $R_3(\tau)$ and $R(\tau)$ follow and at low temperatures are given by

$$R_3(\tau) \underset{\tau \ll 1}{\approx} \frac{1}{\tau}\left[\Delta + \frac{1}{2}\sum_j \chi_j k_j^M\right] + \frac{1}{8}\sum_j \chi_j \ln(c_j^M), \tag{2.24}$$

$$R(\tau) \underset{\tau \ll 1}{\approx} \frac{1}{\tau}\left[1 + \frac{1}{2}\sum_j \gamma_j k_j^M\right] + \frac{1}{8}\sum_j \gamma_j \ln(c_j^M) \tag{2.25}$$

and at high temperatures are given by

$$R_3(\tau) \underset{\tau \gg 1}{\approx} \frac{1}{\tau}\left[\Delta + \frac{1}{2}\sum_j \chi_j \sum_r c_j^{(r)} k_j^{(r)}\right], \tag{2.26}$$

$$R(\tau) \underset{\tau \gg 1}{\approx} \frac{1}{\tau}\left[1 + \frac{1}{2}\sum_j \gamma_j \sum_r c_j^{(r)} k_j^{(r)}\right]. \tag{2.27}$$

(c) The partition function of the Ising model on the kagomé lattice, $Z_{\Lambda_t}(R_3, R, h)$, can be related to the partition function of an equivalent Ising model on the honeycomb lattice, $Z_{G_t}(K, H)$ using two successive transformations: the first one is an inverse star-triangle transformation [7], and the second is a *single* decoration-iteration transformation [22]. As a result of these transformations, we obtain the proportionality relation

$$Z_{\Lambda_t}(R_3, R, h) = \frac{[B(L_1, h_2)]^{3N_t/2}}{[A(L_1, h_1)]^{N_t}} Z_{G_t}(K, H), \tag{2.28}$$

where the partition function of the simple Ising model on the honeycomb lattice is

$$Z_{G_t}(K, H) = \sum_{\{S_i\}_{i \in G_t}} \exp\left\{K \sum_{\langle i,j \rangle \subset C_2} S_i S_j + H \sum_{i \in G_t} S_i\right\}. \tag{2.29}$$

For the first transformation, we obtained the following relations between the parameters [7,8,1]:

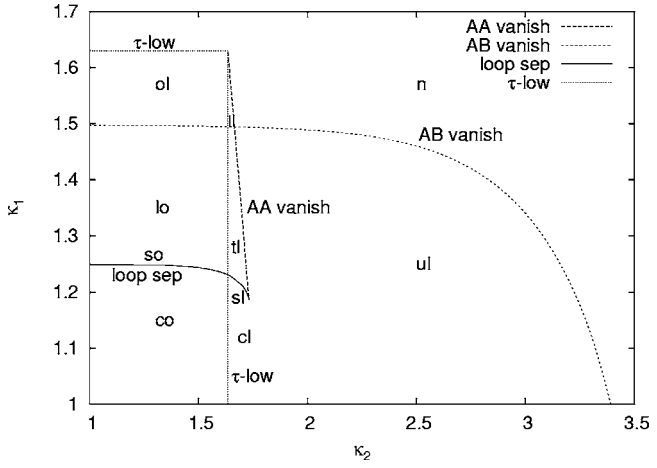

FIG. 3. Domains corresponding to different types of phase diagrams are shown as functions of κ_1 and κ_2, with $q_A=30$, $q_B=3$, $\Delta=0.5$, and $\eta=0.8$. The curves separating domains are denoted as the *loop separation*, the *AA vanish*, *AB vanish*, and τ-*low* curves.

$$\cosh(2L_1) = \frac{e^{4R}+1}{2\sqrt{1-\left[\frac{\sinh(2R_3)}{\sinh(2R)}\right]^2}}, \tag{2.30}$$

$$\cosh(2h_1) = \left\{1+\frac{1}{2}\left[\frac{\sinh(2R_3)}{\sinh(2R)}\right]^2\frac{e^{8R}+3}{e^{4R}-1}\right\} \times\left\{1-\left[\frac{\sinh(2R_3)}{\sinh(2R)}\right]^2\right\}^{-3/2}, \tag{2.31}$$

$$e^{8h_2} = \frac{1-\cosh(2h_1)/\cosh(2L_1)+2\cosh(2L_1-2h_1)}{1-\cosh(2h_1)/\cosh(2L_1)+2\cosh(2L_1+2h_1)}e^{8h}, \tag{2.32}$$

$$A^8 = 2^4[\cosh(6L_1)+\cosh(2h_1)][\cosh(2L_1)+\cosh(2h_1)]^3, \tag{2.33}$$

and the parameters corresponding to the second transformation satisfy the relations

$$\tanh(2h_2) = \frac{\tanh\left[\frac{2}{3}(H-h_1)\right]}{\tanh(2L_1)}, \tag{2.34}$$

$$e^{-2K} = \frac{\cosh\left[\frac{2}{3}(H-h_1)\right]}{\cosh(2L_1)}, \tag{2.35}$$

$$B^4 = 16\cosh(2L_1+2h_2)\cosh(2L_1-2h_2)[\cosh(2h_2)]^2. \tag{2.36}$$

The present model can be extended to describe ternary solutions, in a similar manner as in previous models [1,7]; however, since in the three-component systems there are also *AB* molecules, there are some differences.

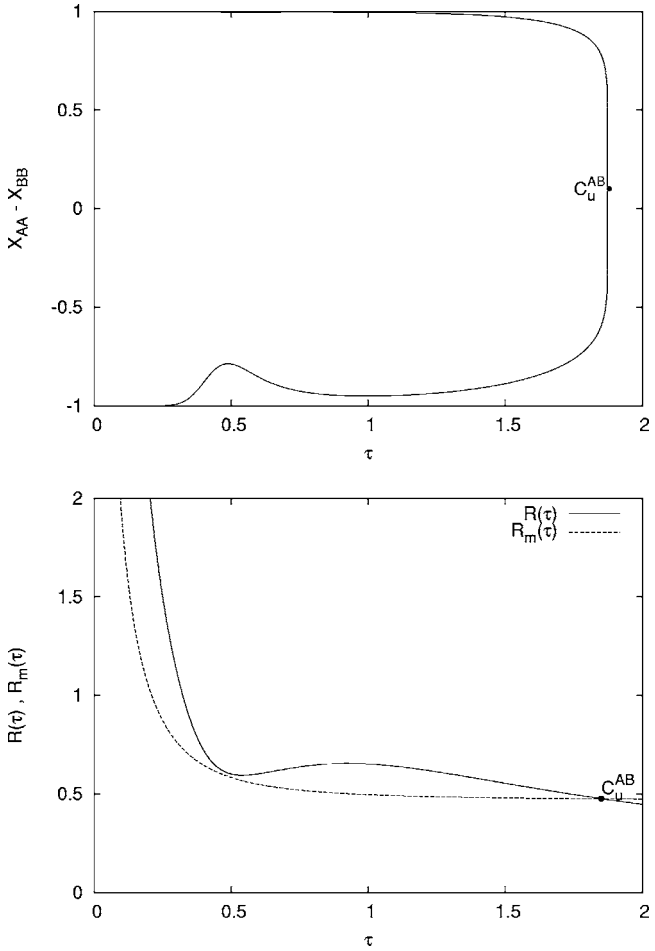

FIG. 4. (a) The phase diagram for $\kappa_1=1.2$ and $\kappa_2=1.2$, corresponding to region co; the compound curve has an upper critical point c_u^{AB} at $\tau_u=1.85021$, $M_u=0.101919$. (b) The plots for $R(\tau)$ and $R_m(\tau)$; at low temperatures $R(\tau)>R_m(\tau)$, and there is only one intersection, corresponding to the upper critical point; also at $\tau\approx0.5$ the two curves are very close to each other, indicating the narrow part of the phase diagram.

(1) The Hamiltonians, expressed by Eqs. (2.6) and (2.9), are similar, but defined on a 3-12 lattice, and the chemical potential μ_{AB} is now included.

(2) The constant K_I in Eq. (2.10) is different.

(3) The exponential in Eq. (2.11) contains a supplementary term $L\Sigma_{\langle i,j\rangle\subset C_2}S_iS_j$, where $L=\beta(\mu_{AA}+\mu_{BB}-2\mu_{AB})/4$, and the corresponding Ising model is defined on a 3-12 lattice.

(4) The first transformation of the Ising model (the inverse star-triangle transformation) is the same for both two-component and three-component systems, giving the relations expressed by Eqs. (2.30)–(2.33). However, the second transformation is now a *double* decoration-iteration transformation and the corresponding new relations between parameters are formally identical with those obtained for the previous models [1,7]; therefore, now the quantity $z=e^{-2K}$ is an independent variable, in contrast to the two-component system, when z satisfies Eq. (2.35).

It is important to observe that all the results for the two-component system can be *formally* obtained from the corre-

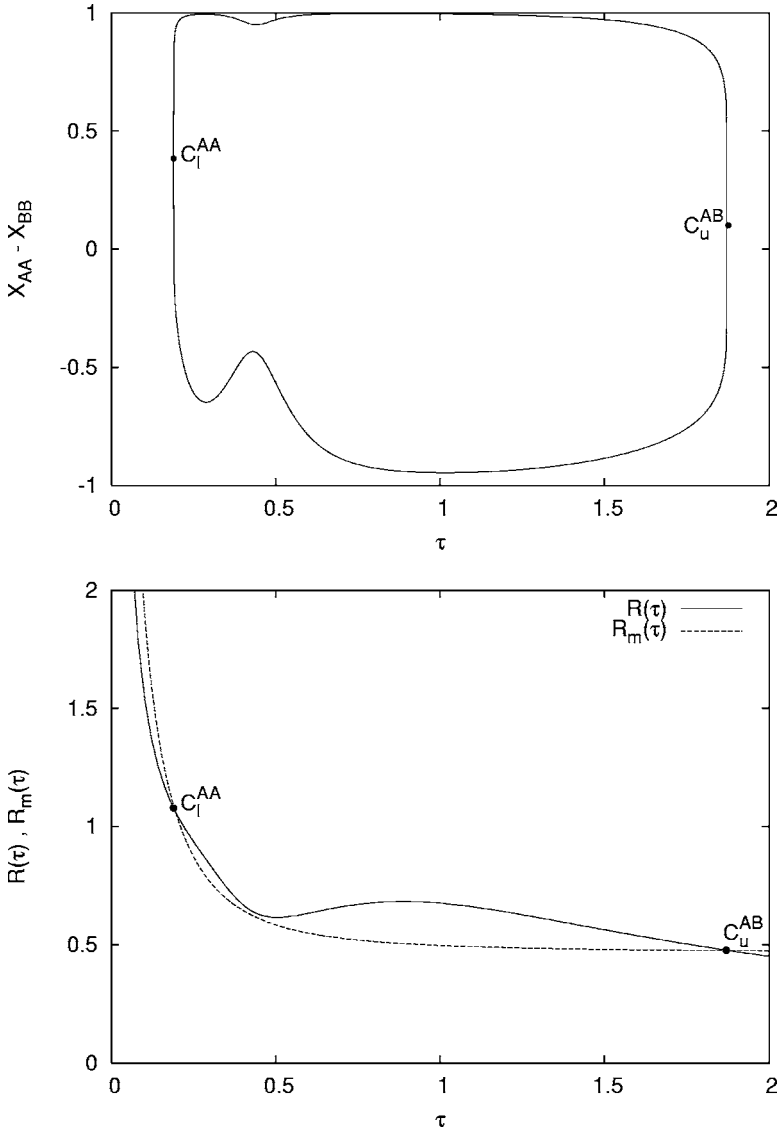

FIG. 5. (a) The phase diagram for $\kappa_1=1.2$ and $\kappa_2=1.7$, corresponding to region cl; the compound closed loop has an upper critical point c_u^{AB} at $\tau_u=1.8695$, $M_u=0.10091$ and a lower critical point c_l^{AA} at $\tau_l^0=0.18861$, $M_l^0=0.383488$. (b) The plots for $R(\tau)$ and $R_{\rm m}(\tau)$; at low temperatures $R(\tau)<R_{\rm m}(\tau)$, showing no phase coexistence. The two curves intersect at the lower and upper critical points; also at $\tau\approx 0.45$ the two curves are very close to each other, corresponding to the narrow part of the phase diagram.

sponding results for the three-component system in the limit $L\to\infty$.

III. EQUATIONS FOR THE PHASE DIAGRAMS

The mole fractions of the binary solution (X_{AA} and X_{BB}) satisfy the conservation equation

$$X_{AA}+X_{BB}=1, \tag{3.1}$$

and their difference is related to the magnetization of the equivalent Ising model on the Λ_∞ lattice in the thermodynamic limit [3,7]:

$$X_{AA}-X_{BB}=M_{\Lambda_\infty}\equiv\langle S_i\rangle_{i\in\Lambda_\infty}. \tag{3.2}$$

In a manner similar to that used in previous papers [1,7,10] for the three-component system, we can express M_{Λ_∞} in terms of the magnetization M_{G_∞} and the spin-spin correlation function σ_{G_∞} of the simple Ising model on the honeycomb lattice:

$$M_{\Lambda_\infty}=\frac{\partial}{\partial h}\lim_{N_t\to\infty}\left.\frac{\ln Z_{\Lambda_t}}{3N_t}\right|_{R_3,R} \tag{3.3}$$

$$=m_0(\tau)+m_s(\tau)\sigma_{G_\infty}(z(\tau))+m_m(\tau)M_{G_\infty}(z(\tau)), \tag{3.4}$$

where the coefficients m_0, m_s, and m_m can be expressed in terms of $a\equiv\cosh(2L_1)$ and $b\equiv\cosh\left[2/3(H-h_1)\right]$:

$$m_0\equiv\frac{1}{2}\left(\frac{\partial\ln B}{\partial h_2}\right)_{L_1}\left(\frac{\partial h_2}{\partial h}\right)_{R_3,R}=\frac{1}{2}\sqrt{\frac{1-1/b^2}{1-1/a^2}}\left(\frac{b^2}{a^2}+1\right), \tag{3.5}$$

$$m_s\equiv\frac{1}{2}\left(\frac{\partial K}{\partial h_2}\right)_{L_1}\left(\frac{\partial h_2}{\partial h}\right)_{R_3,R}=\frac{1}{2}\sqrt{\frac{1-1/b^2}{1-1/a^2}}\left(\frac{b^2}{a^2}-1\right), \tag{3.6}$$

$$m_m\equiv\frac{1}{3}\left(\frac{\partial H}{\partial h_2}\right)_{L_1,h_1}\left(\frac{\partial h_2}{\partial h}\right)_{R_3,R}=\frac{1}{\sqrt{1-1/a^2}}\left(1-\frac{b^2}{a^2}\right). \tag{3.7}$$

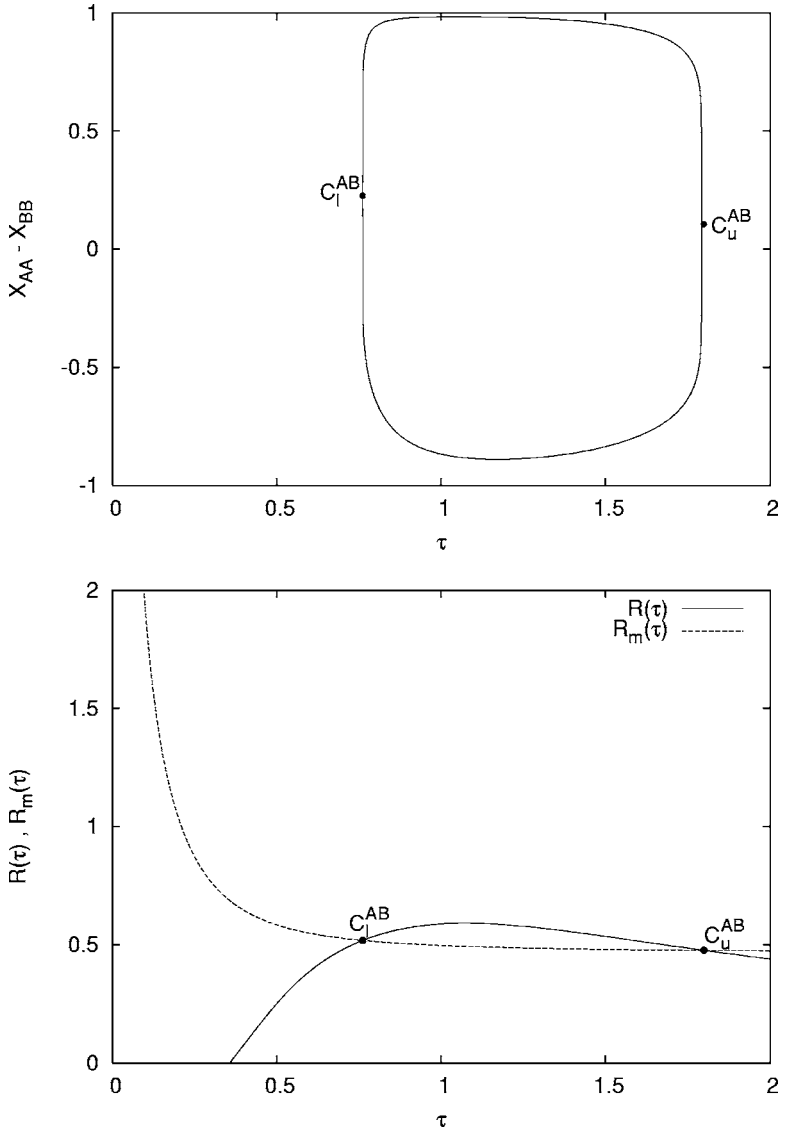

FIG. 6. (a) The phase diagram for $\kappa_1=1.3$ and $\kappa_2=2.0$, corresponding to region ul; here there is only an upper closed loop, having an upper critical point c_u^{AB} at $\tau_u=1.79912$, $M_u=0.104692$ and a lower critical point c_l^{AB} at $\tau_l=0.761058$, $M_l=0.225536$. (b) The plots for $R(\tau)$ and $R_m(\tau)$, showing that $R(\tau)$ has a dominant contribution from the $\overline{AB}$ bonds, which is in accordance with the absence of a lower closed loop; the two curves intersect at the lower and upper critical points.

The simple Ising model on the honeycomb lattice has a ferromagnetic phase transition (when $K>0$) only at zero external field and for sufficiently large values of the coupling constant ($z\equiv e^{-2K}<z_c=2-\sqrt{3}$), so in order to study the phase transition of the binary solution it is necessary to consider only the limit $H=0$. We emphasize that the expressions for the spin-spin correlation function σ_{G_∞} and the magnetization M_{G_∞} for the simple Ising model on the honeycomb lattice at zero external field are well known [23,24], being presented also in our previous papers [1,7,8], so we omit them here.

Using Eqs. (2.30) and (2.31), we observe that a and b in the limit $H=0$ are dependent only on the Ising parameters R_3 and R and thus are functions of the temperature, but these functions depend on the actual model of bonding. Since for some models $R_3(\tau)$ and $R(\tau)$ become infinite at low temperature, it is necessary to extract the divergent part from the coefficients of the magnetization (m_0,m_s,m_m) and also from z, in order to obtain well-defined quantities that characterize the phase transition at the zero-temperature limit (when the system has phase coexistence in this limit).

The domain of temperatures where phase separation occurs is obtained from the condition

$$z(\tau)=\frac{b(\tau)}{a(\tau)}\leqslant z_c, \tag{3.8}$$

and for each temperature inside this domain the phase diagram in the plane $(X_{AA}-X_{BB},\tau)$ has two branches: one corresponding to an AA-rich phase (when M_{G_∞} is positive), the other to a BB-rich phase (when M_{G_∞} is negative), described by Eq. (3.4), and the limiting values $z=z_c$ give the critical points, where the two branches coincide, since $M_{G_\infty}(z_c)=0$.

Because the analytical form of the function $z(\tau)$ is very complicated, it is more convenient to transform the condition (3.8); if we consider $R>0$ (this is a necessary condition) and also $R_3>0$ (since for $R_3<0$ we get similar results), Eq. (3.8) leads to the equivalent condition

$$R(\tau)\geqslant R_m(\tau), \tag{3.9}$$

where the minimum value for R, $R_m(\tau)$, can be given in parametric form:

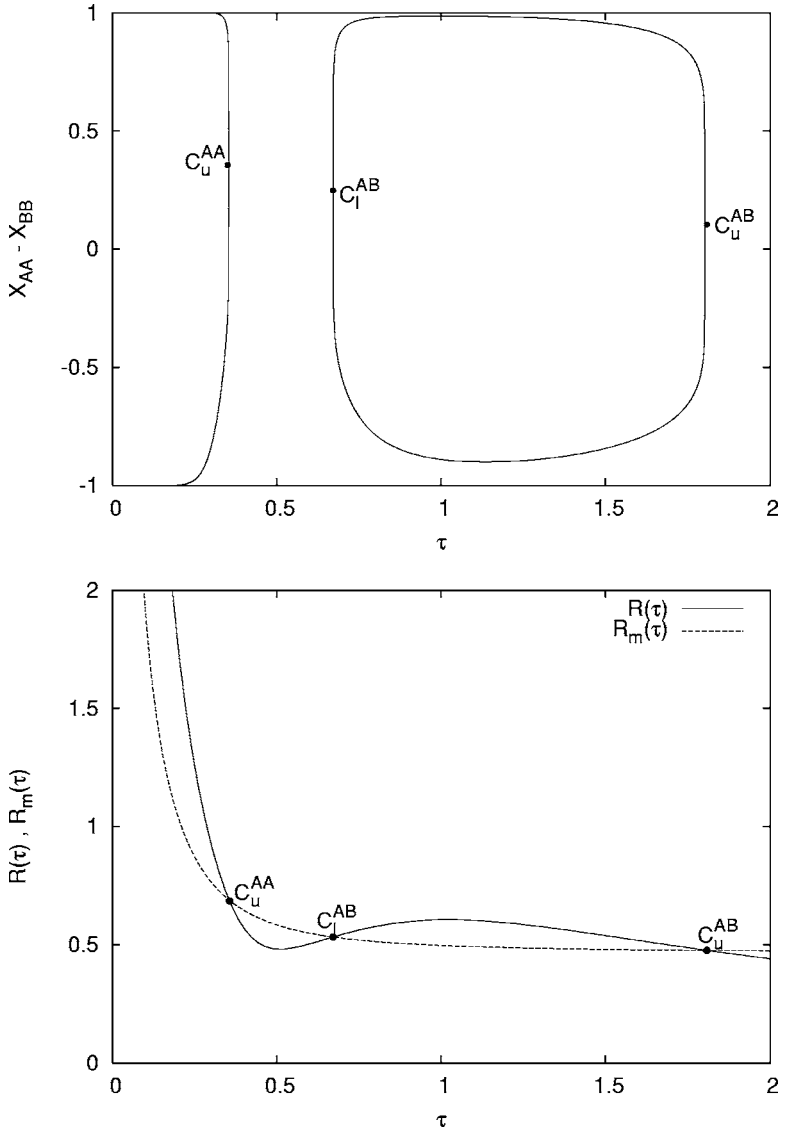

FIG. 7. (a) The phase diagram for $\kappa_1=1.3$ and $\kappa_2=1.2$, corresponding to region Io. There is an upper closed loop with the critical points c_u^{AB} and c_l^{AB} at $\tau_u=1.80775$, $M_u=0.104213$ and $\tau_l=0.671191$, $M_l=0.248104$; also there is a low-temperature open curve with the upper critical point c_u^{AA} at $\tau_u^0=0.355836$, $M_u^0=0.350507$. (b) Plots showing $R(\tau)>R_m(\tau)$ at low and intermediate temperatures, corresponding to the two features of the phase diagram, and three intersections corresponding to the three critical points.

$$\begin{cases} e^{4R_3(\tau)} = 1 + f(x_m) + \sqrt{f^2(x_m) + 2f(x_m)}, \\ e^{4R_m(\tau)} = x_m, \end{cases} \tag{3.10}$$

where $f(x_m)$ is defined as

$$f(x_m) \equiv \frac{(x_m - 1)[z_c(x_m + 1) + 1]^2[z_c(x_m + 1) - 2]}{2x_m[(1 - 3z_c)x_m^2 + 3(1 + z_c)]}.$$

If we consider the case when $R_3(\tau) \to +\infty$ for $\tau \to 0$, then by using the asymptotic behavior, expressed by Eqs. (2.24) and (2.26), and using the notation $C_3 \equiv \Delta + \frac{1}{2}\Sigma_j \chi_j k_j^M$, we obtain the general asymptotic behavior of the function $R_m(\tau)$: (a) at large τ (when $R_3 \to 0$), $R_m(\tau)$ decreases to the limiting value $R_m^0 = \ln(x_m^0)/4$, where $x_m^0 = 2/z_c - 1$, and (b) at low τ (when $R_3 \approx C_3/\tau \to \infty$), $R_m(\tau)$ is also divergent: $R_m(\tau) \approx C_3/(3\tau)$.

The last asymptotic result, together with Eq. (2.24), shows that the phase transition can occur at low temperatures only if $R(\tau)$ is divergent [i.e., it has the form $R(\tau) \approx C/\tau$] and moreover $C_3 < 3C$.

The above results for the two-component system are the same as the results for the corresponding ternary solution (containing AA, BB, and AB molecules) in the limiting case of null values for the mole fraction of AB molecules; in this case, the intersection of the two-phase coexistence surface (in the space $\{\tau, M, X_{AB}\}$) with the plane $X_{AB}=0$ is identical with the phase diagram of the binary solution.

IV. PHASE DIAGRAMS FOR A SIMPLIFIED VERSION OF THE MODEL

The general model contains 16 parameters associated with bonding (the set $k_{XYZ}^{(r)}$): 3 for each AAA and BBB triangle and 5 for each ABA and BAB triangle; also, there are 4 additional parameters: the number of internal states q_A and q_B, the energy ϵ_0 and the asymmetric parameter Δ. Although calculations can be performed with the general model for fixed values of the 20 parameters, we shall instead consider a simplified version of the model that has fewer parameters, but that incorporates the effects of both $\overline{AA}$ and $\overline{AB}$ bonding. The simplifications that define this simplified version of the general model are the following.

(S.1) There are no $\overline{BB}$ bonding states; thus, $\omega_{BBB}=1$.

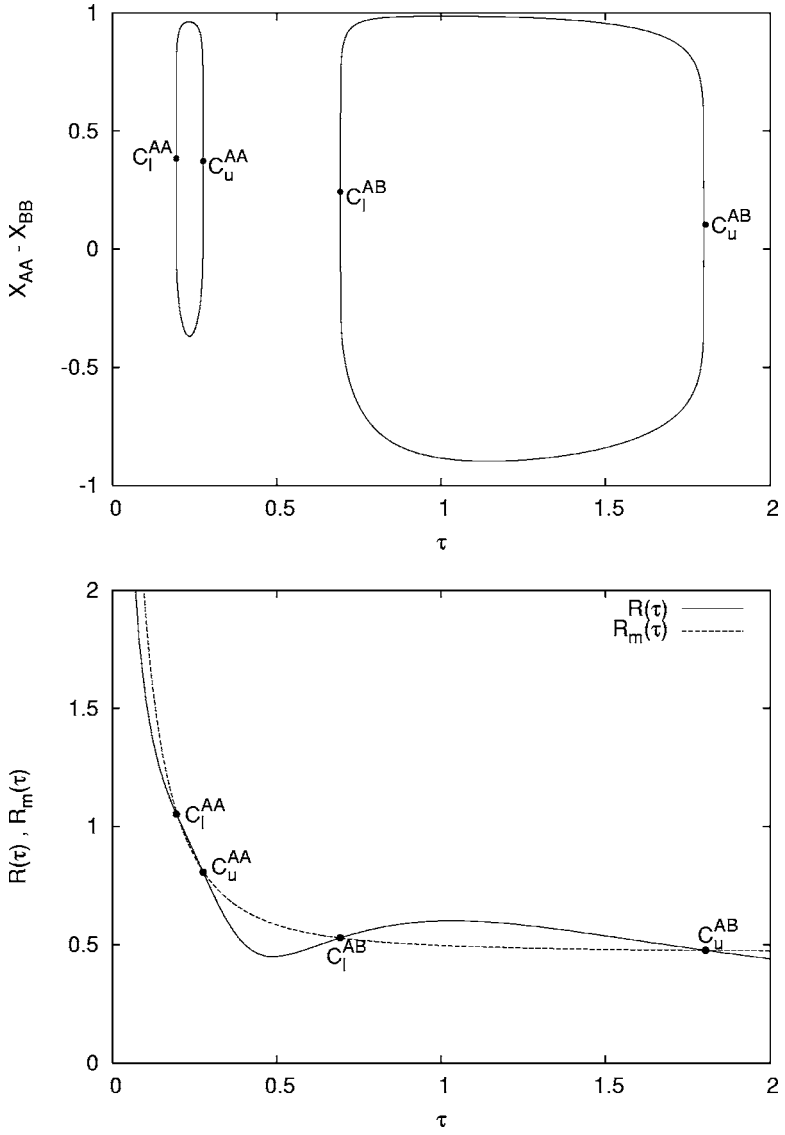

FIG. 8. (a) The phase diagram for $\kappa_1=1.3$ and $\kappa_2=1.7$, corresponding to region tl. There are two closed loops, the upper loop having critical points c_u^{AB} and c_l^{AB} at $\tau_u=1.84347$, $M_u=0.102277$ and $\tau_l=0.581536$, $M_l=0.274169$ and the lower loop having critical points c_u^{AA} and c_l^{AA} at $\tau_u^0=0.337958$, $M_u^0=0.356078$ and $\tau_l^0=0.189678$, $M_l^0=0.383431$. (b) Plots showing that $R(\tau) > R_m(\tau)$ in the domains of temperatures corresponding to the two loops.

(S.2) $\overline{AB}$ bonding energies are the same both in the ABA and BAB triangles, so $\epsilon_{AB}^{(1)}=\epsilon_{BA}^{(1)}\equiv-\epsilon_0\kappa_1$ (for a single $\overline{AB}$ bond) and $\epsilon_{AB}^{(2)}=\epsilon_{BA}^{(2)}\equiv-\epsilon_0\delta$ (for the interaction between two $\overline{AB}$ bonds).

(S.3) $\overline{AA}$ bonds have only two-body interactions; thus, we neglect the interaction energy between two $\overline{AA}$ bonds (in AAA triangles) and neglect also the interaction energy between an $\overline{AA}$ and a $\overline{AB}$ bond (in ABA triangles); in addition, we consider the energy corresponding to an $\overline{AA}$ bond to be the same in AAA and in ABA triangles: $\epsilon_{AA}=-\epsilon_0\eta$.

Using (S.1)–(S.3) and the expressions of the weights given in Tables I and II, we obtain the characteristic function ω_{XYZ} for an XYZ triangle as follows.

In AAA triangles, since there are no interactions between $\overline{AA}$ bonds, the bonding energies are $\delta\varepsilon_{AAA}^{(1)}=-\epsilon_0\eta$, $\delta\varepsilon_{AAA}^{(2)}=-2\epsilon_0\eta$, and $\delta\varepsilon_{AAA}^{(3)}=-3\epsilon_0\eta$; thus, the contribution of the AAA triangles, according to Eq. (2.5), is

$$\omega_{AAA}=\left[\left(1-\frac{1}{q_A^2}\right)+\frac{1}{q_A^2}e^{4\eta/\tau}\right]^3\equiv\left[a_0+a_1e^{4\eta/\tau}\right]^3. \tag{4.1}$$

In BAB triangles, since there are only $\overline{AB}$ bonds (single and double), we can write $\delta\varepsilon_{BAB}^{(1)}=-\epsilon_0\kappa_1$ and $\delta\varepsilon_{BAB}^{(2)}=-\epsilon_0(2\kappa_1+\delta)$. Then the contribution of the BAB triangles is

$$\omega_{BAB}=\left(1-\frac{1}{q_Aq_B}\right)^2+\frac{2}{q_Aq_B}\left(1-\frac{1}{q_Aq_B}\right)e^{4\kappa_1/\tau}+\frac{1}{(q_Aq_B)^2}e^{4(2\kappa_1+\delta)/\tau}\equiv c_0+c_1e^{4\kappa_1/\tau}+c_2e^{4\kappa_2/\tau}, \tag{4.2}$$

where $\kappa_2\equiv2\kappa_1+\delta$.

In ABA triangles, since the $\overline{AA}$ bonding energy is the same as in the AAA triangle and the $\overline{AB}$ bonding energies are the same as in the BAB triangle, we obtain $\delta\varepsilon_{ABA}^{(1;AA)}=-\epsilon_0\eta$ (for an $\overline{AA}$ bond), $\delta\varepsilon_{ABA}^{(1;AB)}=-\epsilon_0\kappa_1$ (for an $\overline{AB}$ bond), $\delta\varepsilon_{ABA}^{(2;AA,AB)}=-\epsilon_0(\eta+\kappa_1)$ (for one $\overline{AA}$ and one $\overline{AB}$ bond), $\delta\varepsilon_{ABA}^{(2;AB)}=-\epsilon_0(2\kappa_1+\delta)$ (for two $\overline{AB}$ bonds), and $\delta\varepsilon_{ABA}^{(3)}=-\epsilon_0(\eta+2\kappa_1+\delta)$ (for an $\overline{AA}$ bond and two $\overline{AB}$ bonds); thus, using Eq. (2.5), we obtain

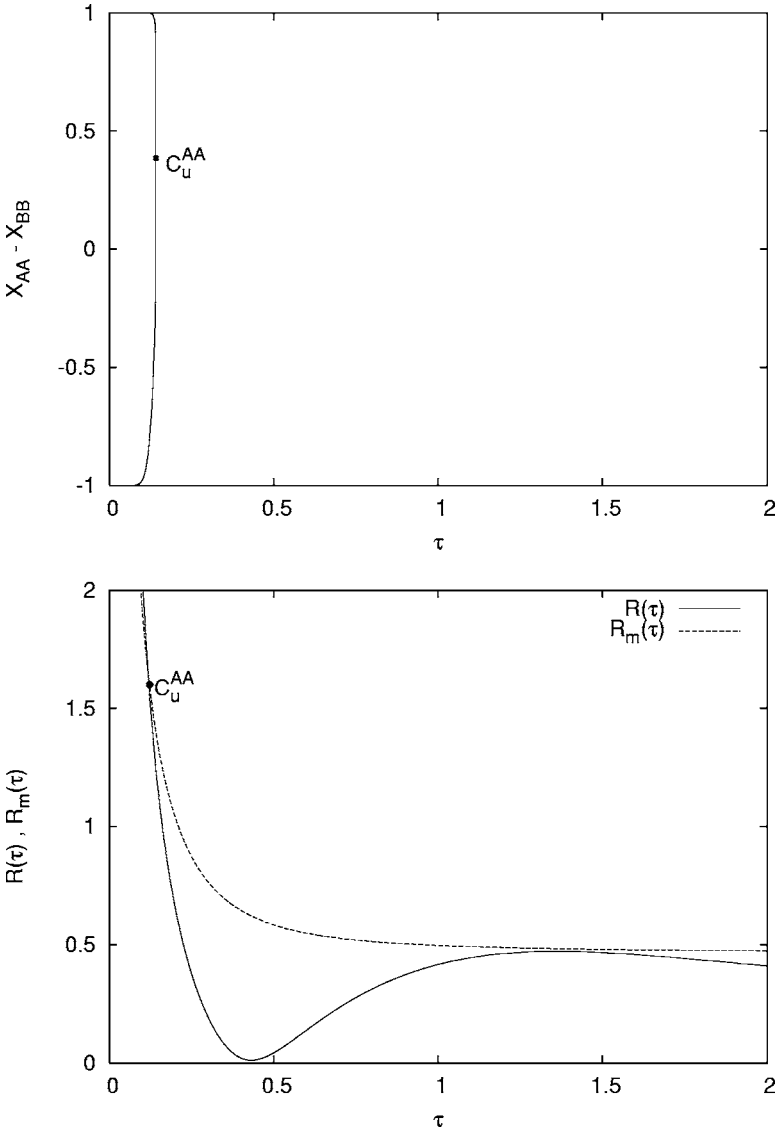

FIG. 9. (a) The phase diagram for $\kappa_1=1.5$ and $\kappa_2=1.2$, corresponding to region OI; here there is only a lower open curve with critical point c_u^{AA} at $\tau_u^0=0.141884$, $M_u^0=0.384762$. (b) Plots showing that at low temperatures, $R(\tau)>R_{\mathrm{m}}(\tau)$, which gives the open curve of the phase diagram. At $\tau \approx 0.4$ the two curves are very close to each other, associated with the collapse of an upper closed loop.

$$\omega_{ABA} = (a_0 + a_1 e^{4\eta/\tau})(c_0 + c_1 e^{4\kappa_1/\tau} + c_2 e^{4\kappa_2/\tau}). \quad (4.3)$$

In this case, according to Eqs. (2.21) and (2.22), we obtain the following expressions for the Ising parameters:

$$R_3(\tau) = \frac{\Delta}{\tau}, \quad (4.4)$$

$$R(\tau) = \frac{1}{\tau} + \frac{1}{4} \ln\left[\frac{a_0 + a_1 e^{4\eta/\tau}}{c_0 + c_1 e^{4\kappa_1/\tau} + c_2 e^{4\kappa_2/\tau}} \right]. \quad (4.5)$$

From Eqs. (4.4) and (4.5), we note that the simplified model has six adjustable parameters: q_A and η associated with $\overline{AA}$ bonding, q_B, κ_1, and κ_2 associated with $\overline{AB}$ bonding, and Δ (together with $\delta=\kappa_2-2\kappa_1$) associated with three-body effects. The effects of $\overline{AA}$ bonding and $\overline{AB}$ bonding on the features of the phase diagram can be investigated by varying the associated parameters. The coexistence curves in a phase diagram can either be open curves ending at $\tau=0$ or closed loops at intermediate temperatures.

To determine whether or not phase separation occurs as $\tau \to 0$, we note that Eq. (4.5) implies $R(\tau)$ tends to zero at high temperatures and at low temperatures

$$R(\tau) \underset{\tau \ll 1}{\approx} \frac{1 + \eta - \kappa_M}{\tau} + \frac{1}{4} \ln\left(\frac{a_1}{c_M} \right), \quad (4.6)$$

where

$$\kappa_M = \max(\kappa_1, \kappa_2) \quad (4.7)$$

and c_M is the coefficient associated with κ_M. The asymptotic behavior of $R_{\mathrm{m}}(\tau)$, derived in Sec. III, together with Eq. (4.4), implies that at low temperatures $R_{\mathrm{m}}(\tau) \approx \Delta/(3\tau)$. Equation (3.9) then implies (for $R_3>0$) that phase separation occurs at low temperatures if

$$0 \leqslant \frac{\Delta}{3} \leqslant 1 + \eta - \kappa_M. \quad (4.8)$$

In order to have dominant contributions at low temperatures from the $\overline{AA}$ bonds and for the $\overline{AB}$ bonds to become important at higher temperatures, we must consider $q_A \gg q_B$

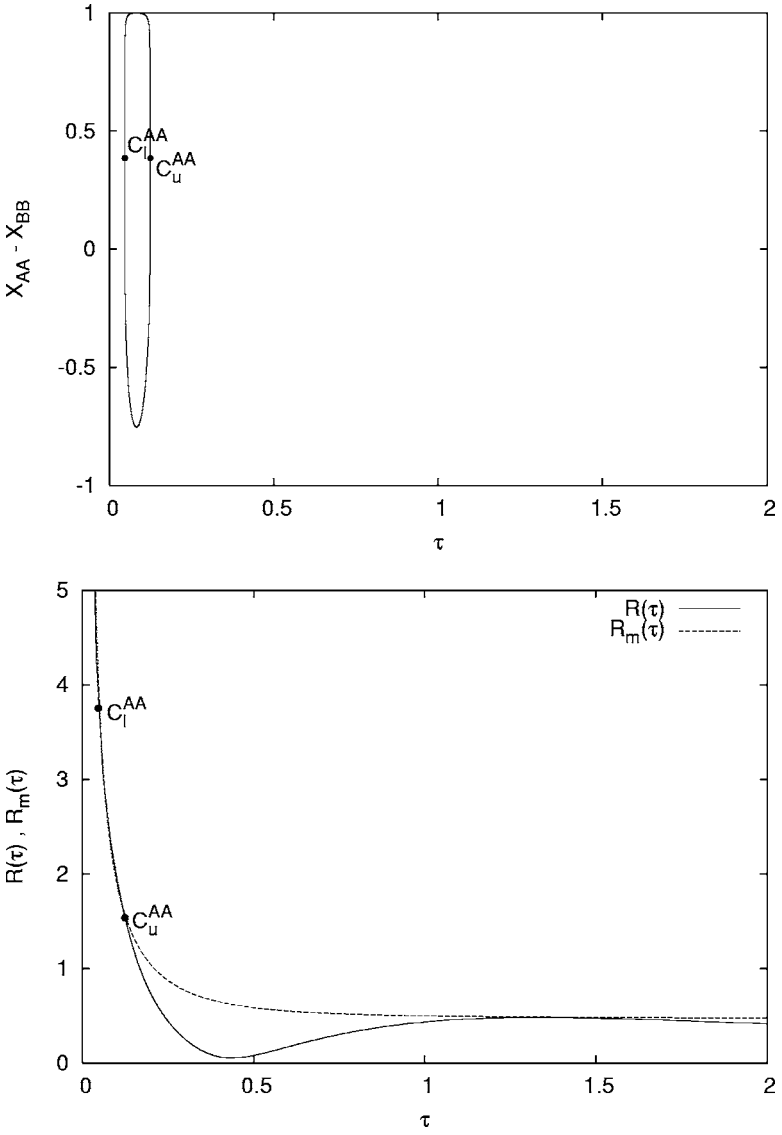

FIG. 10. (a) The phase diagram for $\kappa_1=1.5$ and $\kappa_2=1.65$, corresponding to region II; here the low-temperature part of the phase diagram becomes a closed loop, having critical points c_u^{AA} and c_l^{AA} at $\tau_u^0=0.124333$, $M_u^0=0.384863$ and at $\tau_l^0=0.046858$, $M_l^0=0.3849$. (b) Plots showing that $R(\tau)>R_m(\tau)$ only for $\tau_l^0<\tau<\tau_u^0$. At $\tau\approx 1.5$ the two curves are very close to each other, indicating the collapse of an upper closed loop.

and $\eta<\kappa_M$. Depending on the choice of parameters, the simplified model can exhibit a variety of qualitatively different phase diagrams. In this section we shall illustrate the possible forms of the phase diagrams by considering the following fixed values of the four parameters, $q_A=30$, $q_B=3$, $\Delta=0.5$, and $\eta=0.8$ (these values have been chosen because they produce all the qualitatively different types of phase diagrams), and by varying only the parameters related to the AB bonds (κ_1 and κ_2), considering only values greater than unity since lower values do not produce any qualitatively new situations. For our choice of parameters the limiting value for κ_M, given by Eq. (4.8), is $\kappa_M=1+\eta-\Delta/3=1.633$, when

$$R(\tau)-R_m(\tau)\underset{\tau\to 0}{\to}0,$$

resulting in a critical point at zero temperature.

With the above choice of parameters q_A, q_B, Δ, and η, the phase diagrams can be one of several qualitatively different types. The regions corresponding to each type are illustrated in Fig. 3, and these regions are defined using four curves: the *loop separation*, where the parts of the phase diagram produced by the AA bonds and AB bonds have a common point (the double critical point); the *AA vanish*, where the lower closed loop, produced by the AA bonding, collapses to a point; the *AB vanish*, where the upper closed loop, produced by the AB bonding, collapses to a point; and the *τ-low*, where the lower closed loop has the lower critical point at zero temperature.

In Figs. 4–10 we illustrate examples from each of the eight regions, depicted in Fig. 3, that produce qualitatively different types of phase diagrams. In Figs. 11 and 12 we illustrate two interesting limiting cases of the previous regions.

In order to have a better understanding of the nature of the phase diagrams, we also present plots of $R(\tau)$ and $R_m(\tau)$. Equation (3.9) implies that phase transitions occur only when $R(\tau)>R_m(\tau)$ and the collapse of a closed loop corresponds to a double root of the equation $R(\tau)=R_m(\tau)$. Since $R_m(\tau)$ depends only on Δ and $R(\tau)$ is dependent on η, κ_1, and κ_2, in the displayed plots $R_m(\tau)$ is the same, but $R(\tau)$ differs from plot to plot.

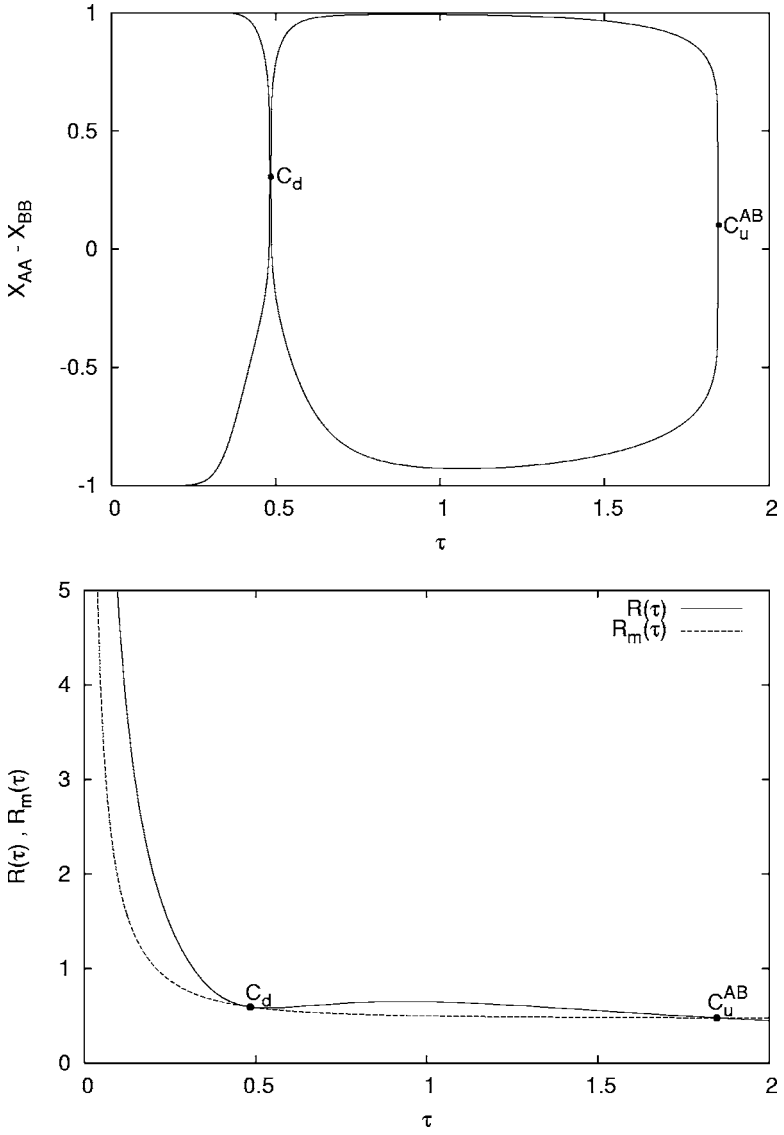

FIG. 11. (a) The phase diagram for $\kappa_1 = 1.2485$ and $\kappa_2 = 1.2$, corresponding to case so. The upper closed loop has an upper critical point c_u^{AB} at $\tau_u = 1.84776$, $M_u = 0.102049$, and it meets the lower open curve at a double critical point c_d at $\tau_d = 0.4849$, $M_d = 0.30605$. (b) Plots showing that $R(\tau) > R_m(\tau)$ for $\tau < \tau_u$ and that at $\tau = \tau_d$ there is a degenerate intersection.

(a) Region co (*compound open*), bordered by the *loop separation* and the *τ-low* curves; the phase diagram has a compound open curve with two branches, starting from zero temperature and ending at the upper critical point, as represented in Fig. 4.

(b) Region cl (*compound loop*), bordered by the *loop separation* (until it reaches the *AA vanish* curve) and the *τ-low* curves, but without a well-defined border with region ul. Here the phase diagram has a compound closed loop, showing a lower and an upper critical point, as is illustrated in Fig. 5.

(c) Region ul (*upper loop*), having as borders the *AA vanish* and *AB vanish* curves, but without a well-defined border with region cl. The phase diagram contains only the upper closed loop, as is represented in Fig. 6.

(d) Region lo (*loop open*), bordered by the *loop separation*, the *AB vanish* and *τ-low* curves. The phase diagram has two parts, an upper closed loop and a lower open curve, as is shown in Fig. 7.

(e) Region tl (*two loops*), bordered by the *loop separation*, the *AA vanish* and *τ-low* curves. The phase diagram has two closed loops, as is illustrated in Fig. 8.

(f) Region ol (*open low*), bordered by the *AB vanish* and *τ-low* curves. Here the phase diagram contains only a lower open curve, as is shown in Fig. 9.

(g) Region ll (*loop low*), bordered by the *AA vanish*, *AB vanish*, and *τ-low* curves. The phase diagram contains only a lower closed loop, as is illustrated in Fig. 10.

(h) Region n (*no phase transition*), bordered by the *AA vanish*, *AB vanish*, and *τ-low* curves (for great values of κ_1 and κ_2). Here there is no phase separation.

In addition, we observe the following two nontrivial limiting cases of the previous regions.

(i) Case so (*separation open*), along the *loop separation* curve with small values for κ_2 (the frontier between regions co and lo), where the upper closed loop and the low-temperature open curve meet at a *double critical point*, as is shown in Fig. 11.

(j) Case sl (*separation loops*), along the *loop separation* curve with greater values for κ_2 (the frontier between regions cl and tl), where the two loops meet at a *double critical point*, as is illustrated in Fig. 12.

There are also some trivial cases, corresponding to the *AA vanish* and *AB vanish* curves, where one closed loop col-

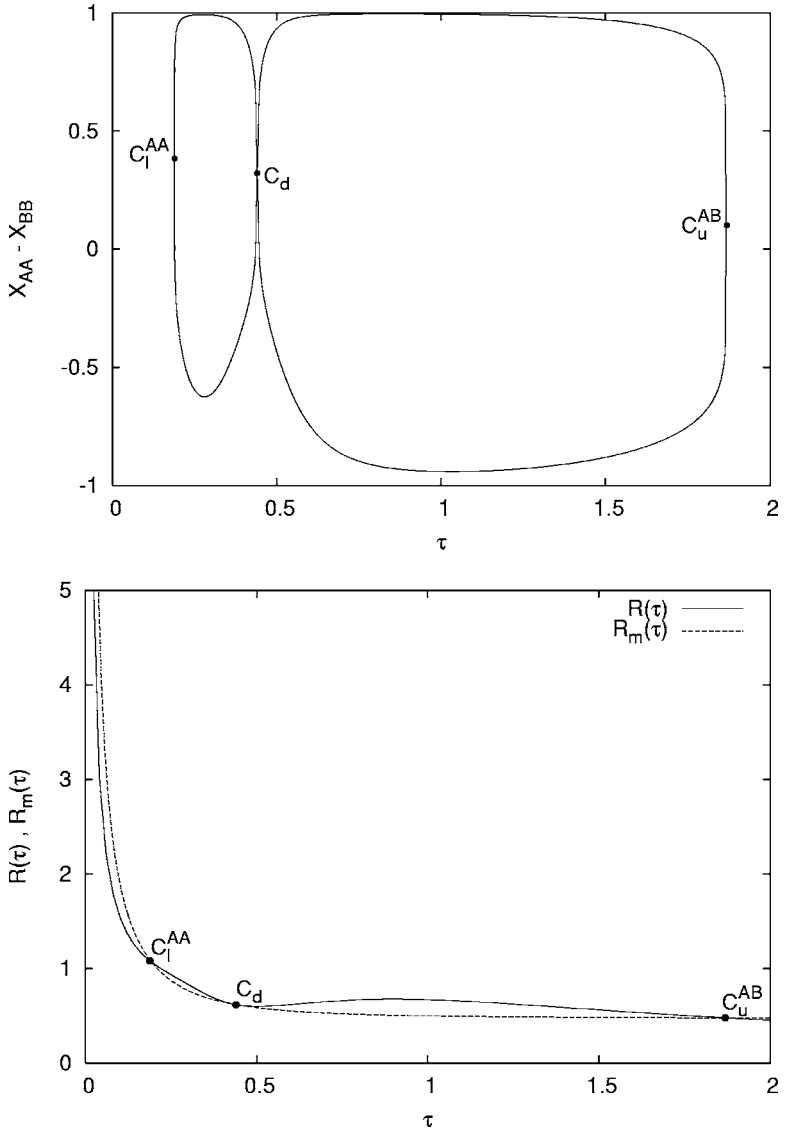

FIG. 12. (a) The phase diagram for $\kappa_1 = 1.2119$ and $\kappa_2 = 1.7$, corresponding to case sl. There are two closed loops that meet at a double critical point c_d at $\tau_d = 0.441$, $M_d = 0.3221$. Also, the upper critical point c_u^{AB} is at $\tau_u = 1.86893$, $M_u = 0.1000939$ and the lower critical point c_l^{AA} is at $\tau_l^0 = 0.188626$, $M_l^0 = 0.383487$. (b) Plots showing that $R(\tau) > R_m(\tau)$ for $\tau_l^0 < \tau < \tau_u$ and that at $\tau = \tau_d$ there is a degenerate intersection.

lapses to a point, or for $\kappa_M = 1.633$, when there is a lower critical point at zero temperature.

We can follow the evolution of the phase diagram, through the different types of domains of phase transitions, by considering some representative fixed values of κ_1 and varying κ_2 (or by fixing κ_2 and varying κ_1).

Taking into account that at low values of κ_2 (which means $\kappa_2 \gtrsim 1$) the curves in Fig. 3 have all almost constant values of κ_1 (for the *loop separation* curve $\kappa_1 \approx 1.25$, for the *AB vanish* curve $\kappa_1 \approx 1.49$, and for the *τ-low* curve $\kappa_1 = 1.633$), we shall vary κ_2 for four representative values of κ_1.

(a) If κ_1 has a value less than that corresponding to the *loop separation* curve (we have chosen $\kappa_1 = 1.2$), then for $\kappa_2 < 1.633$ the phase diagram is an open compound curve corresponding to region co (see Fig. 4). For $\kappa_2 = 1.633$ a compound closed loop appears with a lower critical point at zero temperature. For $1.633 < \kappa_2 < 1.72$ there is a compound closed loop corresponding to region cl (see Fig. 5); then, increasing κ_2 causes the lower loop (produced by the $\overline{AA}$ bonds) to disappear, and for greater values of κ_2 only the upper closed loop remains, corresponding to region ul. Finally, this closed loop (caused by $\overline{AB}$ bonding) shrinks to a point at $\kappa_2 = 3.2243$.

(b) If κ_1 has a value corresponding to the *loop separation* curve (this means $\kappa_1 \approx 1.25$), then for $\kappa_2 < 1.63$ the phase diagram has an upper closed loop and a lower open curve that touch at a double critical point, corresponding to the limiting case so (see Fig. 11). For $\kappa_2 = 1.633$ a lower closed loop appears with the lower critical point at zero temperature. For $1.633 < \kappa_2 < 1.72$ there are two closed loops with a common double critical point, corresponding to the limiting case sl (see Fig. 12); then, as κ_2 increases, the lower closed loop (produced by the $\overline{AA}$ bonds) disappears, and for greater values of κ_2 only the upper closed loop corresponding to region ul remains. Finally, this closed loop (due to $\overline{AB}$ bonding) shrinks to a point at $\kappa_2 = 3.25$.

(c) If κ_1 has a value between those corresponding to the *loop separation* curve and the *AB vanish* curve (we have chosen $\kappa_1 = 1.3$), then for low values of κ_2 ($\kappa_2 < 1.633$) the phase diagram has an upper closed loop and a lower open curve, corresponding to region lo (see Fig. 7). For $\kappa_2 = 1.633$ a lower closed loop appears with a lower critical

point at zero temperature. For $1.633 < \kappa_2 < 1.72$ there are two closed loops, corresponding to region tl (see Fig. 8). Then, as κ_2 increases, the lower open curve (produced by *AA* bonds) disappears. For greater values of κ_2 only the upper closed loop, corresponding to region ul, remains (see Fig. 6). Finally, the closed loop decreases and shrinks to a point at $\kappa_2 = 3.08$ (corresponding to the collapse of the *AB* loop).

(d) If κ_1 has a value greater than that corresponding to the *AB vanish* curve (at low values of κ_2), but less than that corresponding to the *τ-low* curve (we have chosen $\kappa_1 = 1.5$), then for $\kappa_2 < 1.63$ the phase diagram contains only a lower open curve corresponding to region ol (see Fig. 9). For $\kappa_2 = 1.633$ a closed loop appears with a lower critical point at zero temperature, and for $1.633 < \kappa_2 < 1.7$ there is a lower closed loop corresponding to region ll (see Fig. 10). Finally, the closed loop shrinks to a point at $\kappa_2 = 1.71$, corresponding to the collapse of the loop caused by *AA* bonds.

We can also vary κ_1 for 2 representative values of κ_2 that are separated by the value corresponding to the *τ-low* curve (this value is $\kappa_2 = 1.633$), as is seen in Fig. 3.

(a) If $\kappa_2 = 1.2$, for $\kappa_1 < 1.24$ the phase diagram is an open compound curve corresponding to region co (see Fig. 4). For $\kappa_1 = 1.24$ (corresponding to the *loop separation* curve) an upper closed loop forms, joined to the open curve at a double critical point (see Fig. 11). For $1.24 < \kappa_1 < 1.49$ there is an upper closed loop and a lower open curve, corresponding to region lo (see Fig. 7). Then, at $\kappa_1 = 1.49$, the upper closed loop (produced by $\overline{AB}$ bonds) shrinks to a point. For greater values of κ_1 only the lower open curve corresponding to region ol remains (see Fig. 9), and this closed-loop (caused by *AA* bonding) shrinks to a point at $\kappa_1 = 1.633$.

(b) If $\kappa_2 = 1.7$, for $\kappa_1 < 1.25$ (this value of κ_1 corresponds to the *loop separation* curve) the phase diagram has a compound closed loop, corresponding to region cl (see Fig. 5). For $\kappa_1 = 1.25$ loop separation occurs at a double critical point (see Fig. 12). For $1.25 < \kappa_1 < 1.49$ there are two closed loops, corresponding to region tl (see Fig. 8). At $\kappa_1 = 1.49$ (corresponding to the *AB vanish* curve) the upper closed loop (produced by the $\overline{AB}$ bonds) shrinks to a point, and for greater values of κ_1 only the lower closed loop corresponding to region ll remains (see Fig. 10). This closed loop (caused by *AA* bonding) decreases and shrinks to a point at $\kappa_1 = 1.633$.

Thus the simplified version of the model exhibits a rich variety of phase diagrams, containing such features as a double critical point, either one or both of a low-temperature coexistence curve and an intermediate-temperature closed loop, or even two separated closed loops.

ACKNOWLEDGMENT

This research was supported by the Robert A. Welch Foundation, Grant No. P-0446.

[1] F. D. Buzatu, R. P. Lungu, and D. A. Huckaby, J. Chem. Phys. **121**, 6195 (2004).
[2] J. C. Wheeler and B. Widom, J. Am. Chem. Soc. **90**, 3064 (1968).
[3] D. A. Huckaby and M. Shinmi, J. Stat. Phys. **45**, 135 (1986).
[4] D. A. Huckaby, J. Phys. C **19**, 5477 (1986).
[5] M. Shinmi and D. A. Huckaby, J. Phys. A **20**, L465 (1987).
[6] D. A. Huckaby, M. Shinmi, and V. A. Belfi, Physica A **154**, 521 (1989).
[7] D. L. Strout, D. A. Huckaby, and F. Y. Wu, Physica A **173**, 60 (1991).
[8] F. D. Buzatu and D. A. Huckaby, Physica A **299**, 427 (2001).
[9] D. A. Huckaby and M. Shinmi, J. Chem. Phys. **90**, 5675 (1989).
[10] D. A. Huckaby and M. Shinmi, J. Stat. Phys. **60**, 347 (1990).
[11] B. Widom, J. Phys. Chem. **88**, 6508 (1984).
[12] A. Robledo, C. Varea, and E. Martina, J. Phys. (France) Lett. **46**, 967 (1985).
[13] B. Widom, J. Chem. Phys. **84**, 6943 (1986).
[14] C. Varea and A. Robledo, Phys. Rev. A **33**, 2760 (1986).
[15] D. A. Huckaby, A. Pękalski, D. Buzatu, and F. D. Buzatu, J. Chem. Phys. **115**, 6775 (2001).
[16] A. Robledo, Europhys. Lett. **1**, 303 (1986).
[17] A. Robledo, Phys. Rev. A **36**, 4067 (1987).
[18] T. Hoffsäss and H. Kleinert, J. Chem. Phys. **88**, 1156 (1988).
[19] F. D. Buzatu, D. Buzatu, and J. G. Albright, J. Solution Chem. **30**, 969 (2001).
[20] F. Y. Wu and X. N. Wu, Phys. Rev. Lett. **63**, 465 (1989).
[21] X. N. Wu and F. Y. Wu, J. Phys. A **22**, L1031 (1989).
[22] I. Syozi, in *Phase Transitions and Critical Phenomena*, edited by C. Domb and M. S. Green (Academic Press, New York, 1972).
[23] S. Naya, Prog. Theor. Phys. **11**, 53 (1954).
[24] R. M. F. Houtappel, Physica (Amsterdam) **16**, 425 (1950).